Scaling laws for the laser welding process in keyhole mode

Remy Fabbro

PIMM Laboratory (ENSAM-CNRS-CNAM), 151 Boulevard de l'Hôptal, 75013, Paris, France

ARTICLE INFO

Associate editor C.H. Caceres

Keywords:
Keyhole mode laser welding
Keyhole depth
Scaling law
Selective laser melting
Additive manufacturing

ABSTRACT

This study shows that the keyhole model derived for determining the scaling laws of keyhole depths for laser welding when high power incident laser beams are used (typically in the multi-kW incident power range), can be also applied to determine the melted depths observed during the Selective Laser Melting process, where much lower incident powers of typically few hundred watts are focused on very small focal spots. The solution of the thermal analysis of this keyhole configuration is described by only three independent dimensionless parameters that are also involved for the analysis of a more general problem of heat conduction using similar input parameters. This global approach and the keyhole model describing the process of laser welding have been also validated by analyzing the melted depths generated by the Selective Laser Melting process. The dependence of the melted depths on the operating parameters of this process has been established, as well as the formation thresholds of the keyhole.

1. Introduction

Laser welding, which has been used since the 1970s, has become one of the most important laser processes in the industrial world. It allows the assembly of metal parts for a very wide range of thicknesses, from very thick, greater than ten millimeters, thanks to the use of power lasers delivering powers in the multi-kW range, to much smaller thicknesses, less than a millimeter using lasers of much lower power. Many experimental, analytical or numerical studies have made it possible to understand the main physical processes occurring during this very characteristic and complex welding mode, the keyhole (KH) welding, whose melt pool transverse cross sections are characterized by rather large aspect ratios R, defined as the melt pool depth/laser spot diameter (Katayama, 2013). The prediction or the analysis of these KH depths according to the different operating parameters and materials used is therefore of the utmost importance for this application.

In addition, metal addition manufacturing processes, and more particularly the Selective Laser Melting (SLM) of powders, have also become more recently widely used processes (Yap et al., 2015). They produce molten zones of much smaller dimensions, but which can also present the same characteristics of the keyhole mode observed in welding (so with high aspect ratio), whereas the operating parameters used are very different (typically laser incident powers of a few hundred W, laser spot diameters less than 0.1 mm and processing speeds of the order of m/s). Therefore, the occurrence of the KH mode for SLM conditions has been suggested, but never really proven quantitatively, and the knowledge of these melted depths is also very important because the quality of the resulting densification has been shown to be directly related to the melt pool sizes (Tang et al., 2017).

It is the purpose of this article to show that these two very different processes can both be described quantitatively by the same model describing the evolution of the aspect ratio R according to the operating parameters used and the thermo-physical parameters of the material. In a first step, the use of Buckingham's theorem allows to define the number of independent parameters controlling this thermal problem and justifies its solution thus determined, which is recalled. This model is then applied to the analysis of recently published experimental data obtained in SLM conditions, and it is shown that it is possible to reproduce precisely these experimental data as well as the observed thresholds for KH formation.

2. Scaling law methodology

2.1. Definition of the problem

In order to determine the scaling laws that control the KH depth e as a function of the main operating parameters and thermophysical properties of the welded material, several simplifying hypothesis have been used. The KH is assumed to be a vertical cylinder with a diameter d that is equal to the spot diameter of the incident laser beam; this KH is moving with the welding speed V, inside a material at an initial temperature T_0. The incident laser beam is P and A is the fraction of this power absorbed inside the KH. One knows also that the KH walls must have a temperature at least equal to the vaporization temperature T_v;

E-mail address: remy.fabbro@ensam.eu.

So, one will consider that the wall temperature of the cylindrical KH is constant at T_v. The used material is also characterized by its heat conductivity K(W/m.K) and by one of the two last thermophysical parameters: its heat capacity per unit volume ρC_p (J/m^3.K) or its diffusivity κ (m^2/s).

So, in the frame of these hypothesis, one can consider that this problem is totally defined and closed by these previous p = 7 parameters: the resulting KH depth e(m), function of the 3 operating parameters, which are P(W), V(m/s), d(m), the 3 thermophysical parameters: K(W/m.K), ρCp (T/m^3.K) and the KH wall temperature relative to the initial material temperature ($T_v - T_0$)(K). This means that there is a unique relation involving these p = 7 parameters.

Moreover, these 7 parameters are only depending of u = 4 fundamental units, which are the mass [M], the length [L], the time [T] and the temperature [K]. Therefore, the Vaschy-Buckingham π-theorem (Buckingham, 1914) states that under these conditions, there must exist p - u = 3 dimensionless independent parameters (π_1, π_2 and π_3), derived from these initial p parameters, which must satisfy a relation f(π_1, π_2, π_3) = 0.

2.2. Construction of the 3 dimensionless independent parameters

From these 7 initial parameters, 3 dimensionless independent parameters have to be defined (a given dimensionless parameter cannot be derived from another one). There are several possibilities for this construction, by choosing ratios of parameters (or combination of parameters) using for example units of length, velocities, power, power per unit length or volume. A first obvious dimensionless parameter π_1 is the ratio e/d, which is none other than the usually defined aspect ratio R of the KH. A second dimensionless parameter can be defined as $\pi_2 = V\rho C_p\, d/K$, which the ratio of the welding speed V and another velocity such as $K/(\rho C_p\, d)$. In fact one can recognize that this parameter is similar to the well-known Peclet number $Pe = V\rho C_p d/2K$ that will be used below instead. A third dimensionless parameter can be $\pi_3 = P_a/(dK(T_v - T_0)$, which is the ratio of two powers, one is the absorbed laser power $P_a = A\,P$ (with A and P being the absorptivity and the incident power respectively), and the other one results from the combination: $d.K.(T_v - T_0)$.

So the Vashy-Buckingham π-theorem says that it exists one relation between these 3 dimensionless parameters, which could be written as: $\pi_1 = R = F(\pi_3, \pi_2)$.

Now, if one adds that the experimentally observed KH depths are usually proportional to the laser power P, one could finally write:

$$\pi 1 = R = \frac{e}{d} = \pi 3\,.\, f(Pe) = \frac{P_a}{d.\,K.\,(T_v - T_0)}.\, f(Pe) \tag{1}$$

The relation (1) has been obtained only from dimensional analysis, which is rather efficient because it already gives an interesting scaling law with the parameters of this thermal problem. However, a complete dependence with all the involved parameters is not obtained, because the function f(Pe) is not defined here. We will see in Section 3 how f(Pe) can be only obtained from a complete solution of this thermal problem.

2.3. Other possibilities for defining dimensionless parameters

In the previous analysis, the dimensionless parameter $\pi_1 = e/d = R$ is adapted to the process of laser welding in KH mode, because it involves deep penetrations characterized by large KH depths e compared to KH diameters d (i.e. R > 1). But for laser processes involving heat diffusion, (as surface treatments such as laser hardening or surface melting), where the thickness of the affected material has to be determined, a characteristic normalizing dimension that would be more appropriate to this process of heat diffusion, could be some diffusion length δ obtained during the time τ: $\delta = (\kappa.\tau)^{1/2}$, where $\kappa = K/(\rho C_p)$ is the heat diffusivity and $\tau = d/2\,V$ is a characteristic dwell time. So another dimensionless parameter can then be defined such as: $\pi_1' = e/\delta$. One can easily see that π_1 and π_1' are related through the relation:

$$\pi_1' = \pi_1.2Pe^{1/2} \text{ or } e/\delta = 2R.Pe^{1/2} \tag{2}$$

One could also consider another dimensionless parameter $\pi_3' = \Delta H/\Delta h(T)$, which is the ratio of two energy densities, being expressed in J/m^3. This approach was initially used by Hann et al. (2011) for describing the melted depths evolution during laser processing. King et al. (2014) showed that the energy density ΔH represents the energy absorbed A.P.τ during the dwell time τ, which is distributed inside a volume defined by the focal spot diameter and the diffusion length δ: $\pi(d/2)^2\delta$.

This energy density is finally written as $\Delta H = (2^{3/2}\pi)^{1/2}.4.AP.\tau/(\pi.d^2.\delta) = 2^{3/4}AP/(\pi\kappa V(d/2)^3)^{1/2}$ (Rubenchick et al., 2018). (The term $(2^{3/2}\pi)^{1/2}$ was introduced so that ΔH is consistent with the initial definition of Hann et al. (2011)

The second energy density $\Delta h(T)$ can be defined by using the usual enthalpy formulation $\Delta h(T) = \rho C_p.(T - T_0)$. If the laser welding process in the KH mode is analyzed, the enthalpy at vaporization $\Delta h(T_v)$ should be used. But one could also use the enthalpy at the melting $\Delta h(T_m)$, if the melting temperature T_m is the main involved characteristic temperature, as for example in surface treatment.

Similarly to Eq. (2), one has the following relation between π_3' and π_3:

$$\pi_3' = \frac{\Delta H}{\Delta h(T_v)} = (\frac{2^{7/2}}{\pi.\,Pe})^{1/2}.\,\pi_3 \tag{3}$$

Finally, it is also possible to define another energy density ΔH_O (in J/m^3) that is only related to the operating parameters P, V, d such as: $\Delta H_O = AP/(V.d^2)$. Similarly to Eq. (3), a dimensionless parameter $\pi_3'' = \Delta H_O/\Delta h(T_v)$ could be defined. These different dimensionless parameters verify the relation:

$$\pi_3'' = \frac{1}{2Pe}.\pi_3 = (\frac{\pi}{2^{11/2}.\,Pe})^{1/2}.\,\pi_3' \tag{4}$$

The different dimensionless parameters involved in this paper are summarized in Table 1:

3. Solution of this thermal model

3.1. Analysis of high power laser experiments

With the different hypothesis for the KH thermal model defined in § 2.1, it is possible to determine the KH depth resulting from these conditions and compare it with the previous scaling law of Eq. (1). As this determination has already been detailed in a previous publication (Fabbro et al., 2017), the main results will be shortly recalled here.

One considers that the absorbed laser power P_a is homogenously distributed over the KH wall surface at T_v, along the KH depth e. Therefore, if one knows the absorbed power per unit depth $P_z = dP/dz$ that is conducted through the KH wall necessary for maintaining the KH surface at T_v, the KH depth must simply verify the relation $e = P_a/P_z$.

For determining the absorbed power per unit depth $P_z = dP/dz$, we assume a 2D thermal field induced inside the material, because the KH aspect ratio R ≥ 1. Considering stationary conditions, it can be shown that the solution of the 2D heat equation is then only dependent of the

Table 1
Possible dimensionless parameters involved in this thermal problem that depends of the 7 parameters : e(m), P(W), V(m/s), d(m), K(W/m K), ρCp(J/m^3 K), (T_v-T_0)(K). The relations between them are given by the Eqs. (2)–(4).

π_1 (=R) (aspect ratio)	π_2 (=Pe) (Pe number)	π_3	π'_1	π'_3	π''_3
e/d	$V\rho C_p d/2K$	$AP/(dK(T_v$-$T_0)$	e/δ	$\Delta H/\Delta h(T_v)$	$(AP/Vd^2)/\Delta h(T_v)$

Pe number, the KH diameter d and the two temperatures T_v and T_0. As the thermal field is now determined, the resulting heat flux per unit depth P_z conducted through the KH wall can be computed and is then given by:

$$Pz = K.\,(T_v - T_0)\,.\,g(Pe) \tag{5}$$

In Eq. (5), g(Pe) is a function numerically determined of the Pe number. As a result, the aspect ratio R of the KH is then given by:

$$R = \frac{e}{d} = \frac{P_a}{d.\,P_z} = \frac{P_a}{d.\,K.\,(T_v - T_0).\,g(Pe)} \tag{6}$$

By using the independent dimensionless parameters defined in Section 2.3, one can see that the relation (6) can be rewritten as $\pi_1 = \pi_3/g(Pe)$, which is similar to the relation (1); but now the function g(Pe) is determined.

Remark: The absorbed power P_a is related to the incident one P by the relation $P_a = A.P$, where A is the fraction of incident power trapped inside the KH. Due to the cylindrical shape of the KH, the laser beam is absorbed by multi-reflections inside it. The Gouffe (1945) formula takes into account this process and shows that the resulting absorptivity A depends of the aspect ratio R and varies from A_0 for small aspect ratio (typically $A_0 \approx 0.45$, for a metallic surface, with a 1.06 μm wavelength laser) to about 0.8-0.9 for KH's with large aspect ratio R (typically for $R \geq 7$–8). For the analysis of macro-experiments (shown in Fig. 1), where R is large, we will therefore consider that $A \approx 1$; but for SLM micro-experiments, as R is not so important, one should rather consider that $A \approx A_0$.

In order to easily use Eq. (6), we have also shown the great interest in considering that within a given Peclet range, g(Pe) can be assumed to be a linear function of Pe such as: $g(Pe) = m.Pe + n$. The constants m and n are only depending of the considered Pe range (for example, typically $m \approx 2.5$ and $n \approx 3$ for $0.3 < Pe < 10$, which corresponds to the main usual processing conditions for steel alloys, both for laser KH welding or SLM process conditions; for lower Pe, it is observed that m increases and n decreases).

Therefore using this linear relation for g(Pe), Eq. (6) can be re-written as:

$$R = \frac{R_0}{\left(1 + \frac{V}{V_0}\right)} \tag{7a}$$

$$where\ R_0 = \frac{A.\,P}{n.\,d.\,K.\,(T_v - T_0)}\ and\ V_0 = 2\frac{n}{m}\frac{K}{d\,\rho C_p} \tag{7b}$$

Eqs. (7a) and (7b) give the variation of the aspect ratio R as a function of the operating parameters and the thermophysical properties of the material. One can first remark that Eq. 7-a shows a linear dependence of 1/R with the welding speed V; so this behavior should be easily verified for experimental data.

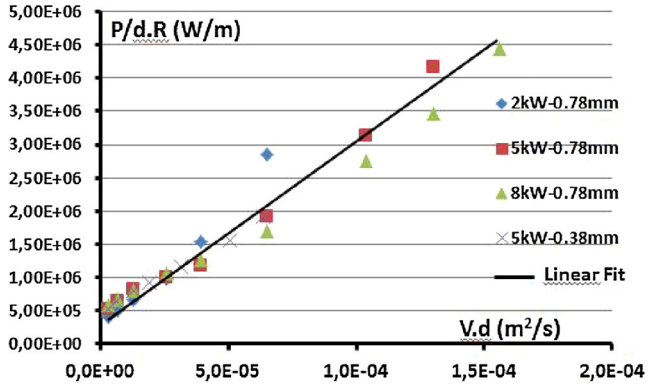

Fig. 1. For St35 steel and different operating parameters (incident powers and focal spot diameters), plot of P/(d.R) as a function of the parameter V.d and corresponding best linear fit (KH depths obtained by Suder and Williams, (2014) at 1.06 μm laser wavelength).

In addition to these previous results, Eq. (7a) can also be rewritten in a more interesting general form, which can be applied with any operating parameters P, V and d and which separates the role of the operating parameters and the thermophysical one:

$$A.P/(d.R) = a + b.(V.d) \tag{8}$$

where

$$a = n.K.(T_v\text{-}T_0) = n.(P/d)_0, \tag{9a}$$

$(P/d)_0 = K.(T_v\text{-}T_0)$ is a characteristic power per unit length necessary for a KH, with the used material,and

$$b = m.(\rho C_p).(T_v\text{-}T_0)/2 = m.\Delta h(T_v)/2 \tag{9b}$$

So for a given material, Eq. (8) shows that for any aspect ratio R resulting of the use of different operating parameters P, V and d, the plot of the variable P/(d.R) as a function of (Vd) is a linear function whose ordinate at origin a and slope b are only depending of the thermophysical properties of the material and the range of the Peclet number (through the m and n dependence). When the range of the welding speed V (or the corresponding Pe number) decreases, as m increases and n decreases, one can see that the ordinate at the origin a decreases and the slope b of the linear function increases.

In Eq. (8), as previously discussed, one can admit that $A \approx 1$, because large aspect ratios are considered here.

This behavior has been verified by analyzing the published data by Suder and Williams (2014) on KH depths obtained on St35 steel at 1.06 μm laser wavelength, for different incident laser powers and focal spots. On Fig. 1, the variable $y = P/(d.R)$ has been plotted as a function of $x = (V.d)$ for these different operating parameters. One sees that the data can be fitted by a unique linear function, $y = a_1 + b_1.x$, with $a_1 \approx 3.0\ 10^5$ W/m and $b_1 \approx 2.6\ 10^{10}$ J/m^3. By considering that $T_v \approx 3100$ K, $T_m \approx 1800$ K, $m \approx 2.5$ and $n \approx 3$ and using Eq. 9, one finds a mean value of $K \approx 40$ W/m.K and $C_p \approx 950$ J/m^3.K, which appears to be rather close to what is expected for this kind of steel (Mills, 2002).

From Fig. 1 it can be seen that the differences between the experimental data and the representative line of the model using realistic thermodynamic parameters are quite small, which can be roughly estimated at about 20% for the large aspect ratios R. This discrepancy seems to increase with the welding speed (or when the aspect ratio R decreases).

One can therefore see that the scaling of the KH depths given by Eq. (7a) (7b)) (or (8)) is verified for these conditions of laser welding at high power and deep KH's. It has also been verified for Cu laser welding (Fabbro et al., 2017), and also for many other data obtained for different operating conditions.

3.2. Analysis of KH mode during selective laser melting additive process

Selective Laser melting (SLM) process uses rather low laser powers (typically several hundred watts) and focused laser beams (typically around 100 μm). It is believed that the depth of the molten pool is controlled by heat conduction in the powder bed and the underlying base material. One also observes for high laser powers (or low scanning speeds) a change in the cross section shape of the molten pool: its melted depth becomes greater than the focal spot diameter, which is characteristic of the KH mode.

This transition from conduction to a KH mode occurs above a threshold that has been analyzed by King et al. (2014). By plotting the melted depth normalized by the beam radius (which is twice the aspect ratio parameter R defined here) as a function of a normalized enthalpy $X = \Delta H/h_s$, they observed a first transition threshold characterizing the melt pool formation for $X_m = \Delta H/h_s \approx 10$; Then, for higher normalized enthalpies, the KH mode appeared typically for a threshold $X_v = \Delta H/h_s$

≈ 25–30. For defining their normalized enthalpy $\Delta H/h_s$, they used the non-dimensional analysis of Hann et al. (2011) where $h_s = \rho C_p T_m$ (h_s is similar to a "melting enthalpy" but rigorously, it differs from the usual h (T_m) melting enthalpy, defined in Section 2.3, because the reference to the initial temperature T_0 of the material is missing; this remark is important if one considers that the initial temperature T_0 may change due to some possible preheating occurrence during the manufacturing process).

Rubenchick et al. (2018) have also reported a more recent analysis of the evolution of these melted depths e as a function of operating parameters for several experiments on steel, Inconel 625 and Ti-6Al-4 V alloys, realized on different machines. They plotted a different normalized depth (e/δ), as a function of the same normalized enthalpy $\Delta H/h_s$, and they showed that all these data could be collapsed in one curve. This result is interesting because it shows that there is a unique mechanism underlying these data obtained for very different machines, operating parameters and materials. As different parameters of particle diameters and layer thicknesses were used, this means that these parameters are not relevant for controlling the melted depths evolution. This can be explained by the fact that the thickness of the powder bed typically used in SLM experiments is about 100 microns (corresponding to 2–3 particle diameters); therefore with a typical density of the powder of about 40-50% of the solid density, this should give a thickness of liquid (or solid) layer of about 40–50 microns, which is rather small compared to the melted depths of about several hundred of microns observed during this process. For the following discussion in Section 3.3, these different normalized data have been reproduced in Fig. 2.

For the analysis of these results, Rubenchick et al. (2018) used a thermal model of the melt pool formation, only based on a conductive process, where the laser beam is absorbed on the planar surface of the sample. With these hypothesis, they showed that the computed melted depth (normalized by δ) is a function of two dimensionless parameters, the previous normalized enthalpy $\Delta H/h_s$, and the inverse of the Peclet number Pe. Of course, this is in agreement with our analysis described in §2, which states that the (normalized) melted depth of this thermal problem only depends of 2 dimensionless parameters. Therefore, the fact that the data shown in Fig. 2 can be collapsed in one curve is rather surprising because it shows a relation between only 2 parameters (the normalized depths and enthalpies), and the dependence with the Peclet number does not seem to appear here. The reason of this behavior will be explained in Section 3.3.

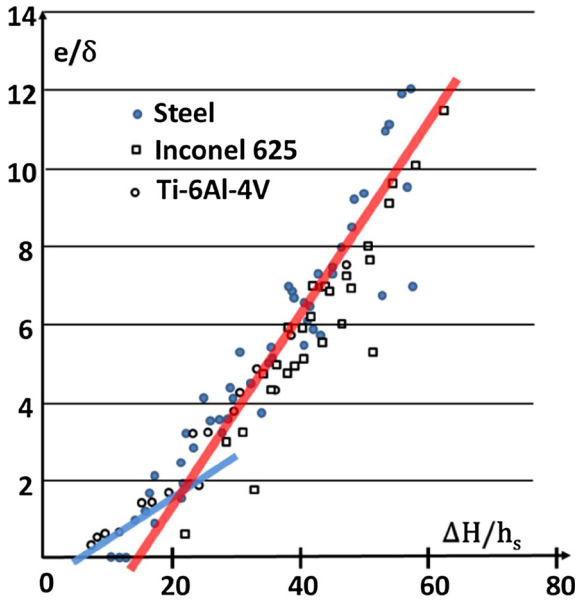

Fig. 2. Normalized melt pool depth e/δ as a function of normalized enthalpy $\Delta H/h_s$ (from Rubenchick et al., 2018 and King et al., 2014). The data for the conduction regime have been fitted with the blue line and those for the KH regime with the red one (For interpretation of the references to colour in this figure legend, the reader is referred to the web version of this article).

Moreover, the use of their thermal model leads to another inconsistency reported by these authors: for high density experiments, leading to observed high aspect ratios characteristic of KH geometries, their simulations show that the peak surface temperature is much greater than T_v. For these conditions, it is clear that a pure conductive model is no more relevant for describing the resulting melt pool shape, because for these high temperatures, the resulting induced recoil pressure strongly deforms the melt pool surface and leads to the usual elongated KH geometry.

However, our approach described in §2 explains the reason for this similarity between the scaling laws derived from a pure conductive model with a planar melt pool surface, and those derived from a cylindrical KH model (and also those derived from experiments, as we will show in the next section). These are the same three independent dimensionless parameters, or others related to them, which can be used for the different solutions describing the thermal field of these two geometries. As discussed in §2, the use of other dimensionless parameters is possible because they are derived from the first three one by relations involving the Pe number.

We will see in the next Section 3.3 how the results described by the Fig. 2, can be reproduced by using a description of a cylindrical KH model that is moving at high velocity.

3.3. *Discussion of the results presented in Fig. 2*

Fig. 2 shows that for SLM processing conditions, the normalized melted depths $Y = e/\delta$ for 3 different alloys, appear to be a function of the normalized enthalpies $X = \Delta H/h_s$ that can be roughly collapsed in one linear curve.

Following the analysis of King et al. (2014), the conduction mode appears for $X > 10$ and the KH mode for $X \geq 25$–30. One can see that it is then possible to fit these experimental points of these two regimes by a linear scaling of the form:

$$Y = Y_0 + \alpha(X - X_0) \tag{10}$$

which have been drawn on Fig. 2.

For the conduction mode, $Y_0 \approx 0$ and $X_0 = X_m \approx 10$ (this value of the threshold X_m can be more easily determined by using the original results of King et al. (2014). Similarly, for the KH mode, using Fig. 2, it is found that $Y_0 \approx 2$ and $X_0 = X_v \approx 25$–30 and also the slope of this linear fit is $\alpha_v \approx 0.25$.

In order to explain these results for the KH mode, we will consider that the melted shape for SLM conditions results from a KH formation whose depth is given by Eq. (7a). But, for usual SLM operating parameters, where typically $V \approx 0.5$–1 m/s, one can verify that $V > > V_0$ (with the heat diffusivity $\kappa \approx 5\ 10^{-6}\ m^2 s^{-1}$, and $d \approx 100\ \mu m$, typically $V_0 \approx 0.12$ m/s and $Pe \geq 5$). Therefore, for these operating conditions, Eq. (7a) can be rewritten as:

$$R = R_0.V_0/V \tag{11}$$

Now, if one expresses the two sides of Eq. (11), by introducing the dimensionless parameters e/δ and $\Delta H/h_s$ used by Rubenchick et al. (2018), one obtains after some manipulations:

$$R = \frac{e}{d} = \frac{e}{\delta}.\ (4Pe)^{-1/2} = \frac{Y}{2.\ Pe^{1/2}} \tag{12}$$

and:

$$R = \frac{R_0 V_0}{V} = \frac{2.\ T_m}{m.\ (T_v - T_0)}.\left(\frac{A.\ P}{V.\ d^2}\right).\frac{1}{h_s} = \frac{\pi^{1/2}}{2^{3/4}}.\frac{1}{2.\ Pe^{1/2}}.\frac{T_m}{m.\ (T_v - T_0)}.\frac{\Delta H}{h_s} \tag{13}$$

Combining Eqs. (12) and (13), one finally finds a linear relation between $Y = e/\delta$ and $X = \Delta H/h_s$, such that $Y = \alpha'.(\Delta H/h_s) = \alpha'.X$, where the slope α' is given by:

$$\alpha' = \frac{\pi^{1/2}}{2^{3/4}}.\frac{T_m}{m.(T_v - T_0)} \tag{14}$$

If one uses $m \approx 2.5$, $T_v \approx 3100$ K, $T_m \approx 1800$ K and $T_0 \approx 300$ K, one obtains $\alpha' \approx 0.27$ from (14). This value appears to be very close to the experimental one derived from the linear fit of Fig. 2, where $\alpha \approx 0.25$.

So, it appears that it is because the Peclet numbers of the corresponding experiments reported in Fig. 2 are large that these data can be collapsed in one curve given by Eq. (11). It also confirms that the melted depths obtained from SLM experiments collected in Fig. 2 for various operating conditions, can be described as resulting from a KH formation, with an adequate thermal field description that considers a KH geometry (This conclusion could already be formulated because of the large aspect ratios commonly observed experimentally of these cross-sections.). Moreover, it is an additional validation of this KH model describing rather small KH's (but nevertheless with rather large aspect ratios) which are obtained for these various SLM operating parameters. Generating a KH under these SLM conditions characterized by high travel speeds is of course possible if one considers that the local intensity of the incident beam is very high (it is typically more than one order of magnitude higher than conventional laser welding). The KH is kept open, with a diameter corresponding approximately to the diameter of the laser spot, only because the very high recoil pressure resulting from this high incident laser intensity balances the surface tension that is very high for these small laser spot diameters.

In addition, because of the high travel speeds during the SLM process and due to the high hydrodynamic velocities induced inside the melt pool, it is observed that the KH no longer remains circular, but is rather elongated in the travel direction (Gunenthiram et al., 2018). In this case it is necessary to compare the heat flux from an elongated KH (typically with an elliptical section) with that from a cylindrical KH. This calculation was performed by Miyazaki and Giedt 1982 and they show that for an elliptical KH the normalized heat flux (always defined by g(Pe)) is higher, due to the larger lateral surface area of the elongated KH, and increases linearly with the parameter (γ-1) (γ is the ratio of the major axis of the ellipse in the travel direction (which therefore increases with the welding speed) and the minor axis of the ellipse, which is about the diameter of the laser spot). Typically for $\gamma \approx 2$ the difference between the two configurations is 17%. As the heat flow is greater with an elliptical KH, the corresponding depth should be lower. However, another effect should reduce this increase. Indeed, the surface temperature of the elongated KH is not uniform at T_v : it is observed that only the front edge of the elongated KH is irradiated by the laser and only this front edge, located under the laser beam, is therefore brought to the vaporization temperature T_v. The rear part of this elongated KH, which is formed by the hydrodynamics of the metallic liquid bypassing the KH front, has a surface temperature that is closer to the melting temperature T_m than T_v. Under these conditions of non-uniform KH wall surface temperature, it is likely that the heat fluxes from these two different KH geometries are comparable. This may explain why these experimental data can be reproduced using the model with a circular KH.

One can also add that for SLM conditions because of the used high welding speeds, the transfer mode of energy inside the SLM sample is dominated by the convective losses compared to conductive losses.

Finally, Eq. (11) can be rewritten in a much more practical equation where the operating parameters are more evidenced. It is easy to see that:

$$R = \frac{R_0 V_0}{V} = \frac{\left(\frac{A.P}{V.d^2}\right)}{0.5 m \rho C_p (T_v - T_0)} = \frac{\Delta H_0}{\Delta h(T_v)'} \tag{15}$$

Eq. 15 shows that the aspect ratio R is equal to the ratio of two energy densities: $\Delta H_0 = AP/Vd^2$ that only contains the operating parameters, and $\Delta h(T_v)' = 0.5\,m.\Delta h(T_v) \approx 0.5\,m.\rho C_p(T_v - T_0)$ is similar to an enthalpy at evaporation temperature (slightly modified through the convective parameter 0.5 m).

3.4. Determination of the threshold X_v

The threshold $X_v \approx 25$–30 for KH generation has been experimentally determined by King et al. (2014). We show here how these results can be derived by using the KH model.

A first usual approach for defining the threshold of KH formation is to determine the operating conditions that induce the evaporation temperature at the surface of the sample. When a laser beam is moving at the surface of a material, the resulting peak temperature T_{max} at the surface is determined by the following relation (Hügel and Graf, 2014):

$$\frac{A.P}{d} = K.(T_{max} - T_0).p.\left(\frac{Pe}{2} + q\right)^{1/2} \tag{16}$$

In (16), $p = \pi/8^{1/2}$ and $q = 4/\pi$ for a Gaussian intensity distribution.

For SLM conditions, as the Peclet numbers Pe are rather large, the relation (16) can be rewritten as:

$$\frac{A.P}{V.d^2} = \frac{\pi}{8}.h_s.\frac{1}{Pe^{1/2}}.\frac{(T_v - T_0)}{T_m} \tag{17}$$

Using (13) and (17), the corresponding threshold X_{v1} can then be estimated:

$$X_{v1} = \frac{\Delta H}{h_s} = \frac{2^2 2^{3/4}}{\pi^{1/2}}.\left(\frac{A.P}{V.d^2}\right).\frac{Pe^{1/2}}{h_s} = \frac{\pi^{1/2}}{2^{1/4}}.\frac{(T_v - T_0)}{T_m} \tag{18}$$

For $T_v \approx 3100$ K, $T_m \approx 1800$ K and $T_0 = 300$ K, one finds $X_{v1} \approx 2.3$, which is quite one order magnitude smaller than the threshold observed experimentally. This means that reaching the evaporation temperature at the surface of the sample, is not a sufficient condition for the KH generation.

One could also consider that a KH can be defined when its aspect ratio R is greater than one. Therefore, our previous result that gives the aspect ratio R as a function of the operating parameters (Eq. (11)) can be used for estimating another threshold X_{v2}. From the condition $R = R_0.V_0/V = 1$, one obtains:

$$\frac{A.P}{Vd^2} = \frac{m.\rho.C_p(T_v - T_0)}{2} \tag{19}$$

The corresponding threshold X_{v2} is then given by:

$$X_{v2} = \frac{\Delta H}{h_s} = \frac{2^2 2^{3/4}}{\pi^{1/2}}.\left(\frac{A.P}{V.d^2}\right).\frac{Pe^{1/2}}{h_s} = \frac{2.2^{\frac{3}{4}}}{\pi^{\frac{1}{2}}}.m.\rho C_p.(T_v - T_0)\frac{Pe^{\frac{1}{2}}}{h_s}$$
$$= \frac{2^{\frac{7}{4}}}{\pi^{\frac{1}{2}}} m \frac{(T_v - T_0)}{T_m} Pe^{\frac{1}{2}} \tag{20}$$

So, also for $T_v \approx 3100$ K, $T_m \approx 1800$ K, $T_0 = 300$ K and $m \approx 2.5$, on finds: $X_{v2} \approx 7.3 Pe^{1/2}$. As for SLM operating conditions we have seen that the Peclet number is rather large (Pe ≈ 5–10), this would correspond to $X_{v2} \approx 16$–23. This range for X_{v2} has a much better agreement than X_{v1} with the experimental determination.

Finally, a third threshold X_{v3} for KH generation can be defined by using an approach based on the analysis of the KH front geometry: for an efficient beam trapping, the KH front inclination must be such that the reflected beam on this front must be redirected downwards, towards the inside of the sample (Fabbro et al., 2017). This KH front inclination at threshold is therefore 45° (this is also roughly equivalent of considering that $R \approx 1$). The condition for obtaining an inclination angle of 45° has already been estimated (Fabbro et al., 2017), and is given by the relation:

$$\frac{A.P}{Vd^2} = \frac{\pi.H_0}{4} \tag{21}$$

where H_0 is a modified melting enthalpy derived from the piston model (Semak and Matsunawa, 1997) that takes into account also some losses by heat diffusion. Using (21), the corresponding threshold X_{v3} is then:

$$X_{v3} = \frac{\Delta H}{h_s} = \frac{2^2 2^{3/4}}{\pi^{1/2}} . \left(\frac{A . P}{V . d^2}\right) . \frac{Pe^{1/2}}{h_s} = 2^{3/4}\pi^{1/2} . \frac{H_0}{h_s} . Pe^{1/2} \quad (22)$$

For the considered range of the Peclet number, it can be shown that $H_0/h_s \approx 2$. So (22) gives:

$$X_{v3} \approx 6.Pe^{1/2} \approx 0.8\ X_{v2} \quad (23)$$

For defining the KH formation threshold, Eq. (23) shows that the two very different approaches give similar results, which are quite close to the experimental threshold determination. It also means that reaching the evaporation temperature at the surface of the sample, defined by the threshold X_{v1}, is not a sufficient condition to generate a KH during these SLM operating conditions. The laser intensity should be increased in order to induce a significant depression of the melt pool.

4. Conclusions

In this study, using an approach based on energy conservation of the absorbed power inside a cylindrical KH, an analytical model has been developed that gives the evolution of the KH depth as a function of the operating parameters and the thermophysical data of the used material. The main results can be summarized as follows:

- As a general law, it is obtained that the inverse of the KH depth appears to be a linear function of the welding speed. This point is always verified by corresponding experiments.
- The effects of all the operating parameters and thermophysical data of the used material have been clarified. The resulting KH depths obtained with multi-kW lasers can be predicted with a rather good agreement by this model, and it should be considered as an interesting tool in an industrial environment.
- It has also been shown that the melted depths observed during the Selective Laser machining process for different operating conditions and materials, can be reproduced using the same KH model. This implies that the involved SLM process can be quantitatively and definitively interpreted as a KH mode welding.
- This KH model defines the conditions for achieving the threshold for KH formation. It is shown that the occurrence of the evaporation temperature at the sample surface is not a sufficient condition for achieving this threshold.

Declaration of interest

None

Acknowledgments

I acknowledge fruitful discussions with Patrice Peyre, Morgan Dal and Matthieu Schneider. This work was performed under the auspices of the Centre National de la Recherche Scientifique (CNRS) at the PIMM laboratory.

References

Buckingham, E., 1914. On physically similar systems. Illustrations of the use of dimensional equations. Phys. Rev. 4 (4), 345–376.

Fabbro, R., Dal, M., Peyre, P., Coste, F., Schneider, M., Gunenthiram, V., 2017. Analysis and possible estimation of keyhole depths evolution, using laser operating parameters and material properties. LIA (Ed.), Proceedings of ICALEO 801–809.

Gouffe, A., 1945. Correction d'ouverture des corps noirs artificiels compte tenu des diffusions multiples internes. Revue d'Optique 24, 1–10.

Gunenthiram, V., Peyre, P., Schneider, M., Dal, M., Coste, F., Koutiri, I., Fabbro, R., 2018. Experimental analysis of spatter generation and melt-pool behavior during the powder bed laser beam melting process. J. Mater. Process. Technol. 251, 376–386.

Hann, D.B., Iammi, J., Folkes, J., 2011. A simple methodology for predicting laser-weld properties from material and laser parameters. J. Phys. D Appl. Phys. 44, 445401.

Hügel, H., Graf, T., 2014. Laser in der Fertigung, third ed. Springer, pp. 167 978-3-8348-1817-1.

Katayama, S., 2013. Introduction: fundamental of laser welding. In: Katayama, S. (Ed.), Handbook of Laser Welding Technologies. Woodhead Publishing Limited, Cambridge, UK, pp. 3–16.

King, W.E., Barth, H.D., Castillo, V.M., Gallegos, G.F., Gibbs, J.W., Hahn, D.E., Kamath, C., Rubenchik, A.M., 2014. Observation of keyhole-mode laser melting in laser powder-bed fusion additive manufacturing. J. Mater. Process. Technol. 214, 2915–2925. https://doi.org/10.1016/j.jmatprotec.2014.06.005.

Mills, K.C., 2002. Recommended Values of Thermophysical Properties for Selected Commercial Alloys. Woodhead Publishing Limited, Abington Cambridge, UK.

Miyazaki, T., Giedt, W.H., 1982. Heat transfer from an elliptical cylinder moving through an infinite plate applied to electron beam welding. Int. J. Heat Mass Transf. - Theory Appl. 25 (6), 807–814.

Rubenchick, A.M., King, W.E., Wu, S.S., 2018. Scaling laws for additive manufacturing. J. Mater. Process. Technol. 257, 234–243.

Semak, V., Matsunawa, A., 1997. The role of recoil pressure in energy balance during laser materials processing. J. Phys. D Appl. Phys. 30 (18), 2541–2552. https://doi.org/10.1088/0022-3727/30/18/008.

Suder, W.J., Williams, S., 2014. Power factor model for selection of welding parameters for CW laser welding. Opt. Laser Technol. 56, 223–229.

Tang, M., Pistorius, P.C., Beuth, J.L., 2017. Prediction of lack-of-fusion porosity for powder bed fusion. Addit. Manuf. 14, 39–48.

Yap, C.Y., Chua, C.K., Dong, Z.L., Liu, Z.H., Zhang, D.Q., Loh, L.E., Sing, S.L., 2015. Review of selective laser melting: materials and applications. Appl. Phys. Rev. 2 (2015), 041101. https://doi.org/10.1063/1.4935926.